

The influence of experimental and sampling uncertainties on the probability of unsatisfactory performance in geotechnical applications

D. Mašín

Charles University in Prague

Faculty of Science

Albertov 6

12843 Prague 2, Czech Republic

E-mail: masin@natur.cuni.cz

Tel: +420-2-2195 1552, Fax: +420-2-2195 1556

Number of words, main text: 4790

Number of words, total: 5870

Number of tables: 1

Number of figures: 16

August 23, 2015

Manuscript accepted for publication in Géotechnique

1 Abstract

While the effect of spatial variability on the probability of unsatisfactory performance in geotechnical applications is relatively well understood, comparatively less attention has been given in the literature to the effects of experimental (measurement scatter) and sampling (insufficient number of samples) uncertainties. In this paper, a general approach is developed to incorporate experimental and sampling uncertainties into probabilistic analyses based on random field methods. It is shown that, when compared with the standard approach which attributes the measured total soil variability to spatial variability, consideration of experimental uncertainty may significantly reduce the calculated probability of unsatisfactory performance. It is argued that this may be one of the reasons for an overestimation of the probability of unsatisfactory performance in geotechnical probabilistic simulations (another important reason is the spatial averaging of soil properties). Evaluation of the sampling uncertainty reveals that, although a relatively large number of samples is needed for spatial variability characterisation, a limited number of samples is sufficient to quantify the experimental uncertainty. It is pointed out that no adjustments of the existing random field-based software are needed to consider the additional uncertainties. To illustrate the proposed approach, two extensive experimental data sets on sand are presented: one reflecting total variability and the other quantifying experimental uncertainty. A hypoplastic model is calibrated against the two data sets and adopted in random field analyses of strip footing settlement.

Keywords: probabilistic methods; random field method; experimental uncertainty; sampling uncertainty; constitutive model; sand.

Introduction

Design parameters obtained from any geotechnical site investigation are subject to uncertainties. These are caused, in particular, by (a) an inherent spatial variability of soil properties, (b) experimental uncertainty (measurement scatter) due to limitations of the experimental techniques and (c) sampling uncertainty (statistical uncertainty) due to the limited number of soil samples used in the investigation (Phoon & Kulhawy (1999a), Schweiger & Peschl (2005), Christian *et al.* (1994)). Other uncertainty sources, which are not within the scope of this paper, involve transformation uncertainty (transformation of the measured value to the design value by means of a potentially inaccurate empirical method), material model uncertainty (imperfect representation of soil behaviour by a material model) and experimental bias (systematic measurement error due to problematic functioning or calibration of the experimental device).

Formal treatment of the *spatial variability* is relatively well understood, as it has been studied

thoroughly in the geotechnical literature. Spatial variability has been investigated experimentally (e.g., Suchomel & Mašín (2011), Zhao *et al.* (2013), Akbas & Kulhawy (2010), Wang & Chiasson (2006), Hicks & Onisiphorou (2005), Kim (2002), Lumb (1966), Soulié *et al.* (1990), Jung *et al.* (2008), El-Ramly *et al.* (2005), El Gonnouni *et al.* (2005), Elkateb *et al.* (2003)), treated formally using random-field methods (e.g., Vanmarcke (1983), Griffiths & Fenton (2004), Suchomel & Mašín (2010), Suchomel & Mašín (2011), Nübel & Karcher (1998), Andrade *et al.* (2008), Cho & Park (2010), Niemunis *et al.* (2005), Kim & Santamarina (2008), Hsu & Nelson (2006)) or by using approximate probabilistic methods involving spatial averaging of soil properties (e.g., Suchomel & Mašín (2010), Suchomel & Mašín (2011), Brzakała & Puła (1996), Peschl & Schweiger (2003), Cho (2007), El-Ramly *et al.* (2002)). It has been shown that the spatial correlation significantly affects the results of probabilistic analyses of various geotechnical problems (e.g., Wang & Chiasson (2006), Hicks & Onisiphorou (2005), Nour *et al.* (2002), Fenton & Griffiths (2002), Fenton & Griffiths (2005), Huber *et al.* (2010), Griffiths *et al.* (2002), Fenton & Griffiths (2003), Hicks & Samy (2002), El-Ramly *et al.* (2006), Haldar & Babu (2008), Popescu *et al.* (1997)).

Less attention has been paid to the other uncertainty sources. An additive model separating different uncertainties has been proposed by Phoon & Kulhawy (1999b). They considered the reduction of spatial variability using a spatial averaging factor (Vanmarcke, 1983) and additively included variance due to experimental uncertainty in the global parameter variance. However, this may lead to an overestimation of the global uncertainty; this issue is discussed in detail later in this paper and was also implied by Müller *et al.* (2014). A similar simplified approach has been followed by Akbas & Kulhawy (2010) and by Al-Naqshabandy & Larsson (2013), who also included the effects of sampling and transformation uncertainties. A general approach to uncertainty quantification, including a proper treatment of the experimental uncertainty, was presented by Christian *et al.* (1994) and Müller *et al.* (2014); they did not consider random field characterisation of spatial variability, but instead adopted a simpler method based on spatial averaging. Another approach to quantify the effect of experimental uncertainty is represented by the theory of random sets, applied to geomechanical problems by Schweiger & Peschl (2005) and Oberguggenberger & Fellin (2008). More publications on separating different uncertainty sources can be found in the field of hydrology (Merz & Thielen (2005), Sun *et al.* (2012), Booy & Lye (1989)) and other engineering disciplines (Castrup (2004), Frey (1993), Helton (1997)). From an experimental perspective, experimental uncertainty can, in principle, be estimated by quantifying the variations in repeated measurements of the same property on identical soil samples. As pointed out by Akbas & Kulhawy (2010), however, very few studies of this kind can be found in the geotechnical literature. Statistical evaluation of experiments on a relatively uniform 1m clay sample was presented by Watabe *et al.* (2007). An experimental characterisation of sampling uncertainty has been presented by Bourdeau & Amundaray (2005) and Wu *et al.* (2013).

In this paper, a general approach is developed to incorporate spatial variability and experimental

and sampling uncertainties into geotechnical analyses based on the random field method. Subsequently, extensive experimental data sets on both the spatial variability and experimental uncertainty are presented and the proposed approach is demonstrated by simulation of a typical geotechnical problem; the settlement of a strip footing.

Incorporation of experimental uncertainty

In this section, it is assumed that the global variability and the experimental uncertainty are known exactly. That is, the sampling uncertainty is neglected, which will be covered later. It is assumed that the following two measurement data sets are available:

- Measurements in the spatial grid aimed at evaluating spatial variability for random field probabilistic analyses. These measurements contain information on the spatial variability. Inevitably, however, the data from each spatial node are themselves subject to the experimental uncertainty.
- Repeated measurements on nominally identical samples to quantify the experimental uncertainty.

Let us denote the uncertain parameters as X_i (where i is the parameter number). $X_1, X_2 \dots X_n$ may represent, for example, parameters of the constitutive model (such as friction angle and cohesion), or uncertain values of the state variables (such as the void ratio).

Calculation of spatial variability by extracting the experimental uncertainty from the total variability

The value of the parameter X_i , which depends on spatial position \mathbf{x} , can be written as

$$X_i(\mathbf{x}) = \mu[X_i](\mathbf{x}) + \varepsilon_t[X_i](\mathbf{x}) \quad (1)$$

where $\mu[X_i](\mathbf{x})$ is the mean value of the parameter X_i at the given position \mathbf{x} and $\varepsilon_t[X_i]$ is the stochastic component which lumps different sources of uncertainty (subscript t stands for "total"). In the following, the spatial variation is considered a spatially random process without any trend in the dependency of $\mu[X_i]$ by location. That is, the mean value $\mu[X_i]$ is considered as a constant, and the total variability component is represented by $\varepsilon_t[X_i]$ with zero mean value. Thus,

$$X_i(\mathbf{x}) = \mu[X_i] + \varepsilon_t[X_i](\mathbf{x}) \quad (2)$$

The total variability is (in this section) composed of two components: spatial variability ε_n (subscript n for "natural") and experimental uncertainty ε_e (subscript e for "experimental"). ε_n depends on the spatial location \mathbf{x} , whereas the experimental uncertainty is assumed to be independent of location. Therefore:

$$\varepsilon_t[X_i](\mathbf{x}) = \varepsilon_n[X_i](\mathbf{x}) + \varepsilon_e[X_i] \quad (3)$$

and

$$X_i(\mathbf{x}) = \mu[X_i] + \varepsilon_n[X_i](\mathbf{x}) + \varepsilon_e[X_i] \quad (4)$$

As the mean value of $X_i(\mathbf{x})$ is constant, and $\varepsilon_n[X_i](\mathbf{x})$ and $\varepsilon_e[X_i]$ are independent variables, variance of $X_i(\mathbf{x})$ is calculated as:

$$\text{var}[X_i(\mathbf{x})] = \text{var}[\varepsilon_t[X_i](\mathbf{x})] = \text{var}[\varepsilon_n[X_i](\mathbf{x})] + \text{var}[\varepsilon_e[X_i]] \quad \forall \mathbf{x} \in R \quad (5)$$

where R is the area of interest, representing, for example, a geological layer with given parameter statistics. For brevity, statistical variables in this section always represent parameters X_i and the notation can be simplified as $\varepsilon_t[X_i] = \varepsilon_t$. Therefore:

$$\text{var}[\varepsilon_t(\mathbf{x})] = \text{var}[\varepsilon_n(\mathbf{x})] + \text{var}[\varepsilon_e] \quad \forall \mathbf{x} \in R \quad (6)$$

which allows us to calculate the variance due to the spatial variability from the known total variance and variance due to the experimental variability as

$$\text{var}[\varepsilon_n(\mathbf{x})] = \text{var}[\varepsilon_t(\mathbf{x})] - \text{var}[\varepsilon_e] \quad \forall \mathbf{x} \in R \quad (7)$$

For text brevity, the spatial position identified \mathbf{x} will be omitted in the following text.

Quantification of spatial correlation properties for zero experimental uncertainty

Probabilistic analyses that consider the spatial variability of material properties often make use of so-called *random field* methods. These methods are based on spatial statistics of the input parameters, which are adopted to generate a random field. Statistical characteristics of the performance function (model output) can then be evaluated using methods such as Monte-Carlo, which involve a number of random field realisations.

A random field can be characterised by the statistical distribution of the input parameter and by the dependency between measurements of the parameter at two locations on the separation distance. This dependency may be described by a *semi-variogram*¹ $\gamma_v(\tau)$. An empirical semi-variogram can

¹To avoid confusion with the variance reduction factor γ , the semi-variogram is in this paper denoted as γ_v in place of the standard notation γ .

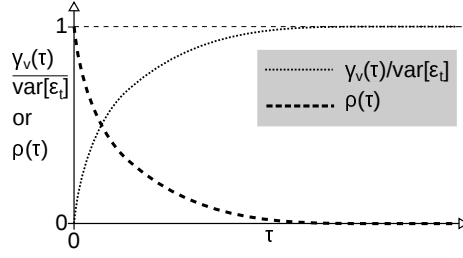


Figure 1: Normalised semi-variogram and correlogram for zero experimental uncertainty ($\text{var}[\varepsilon_e] = 0$).

be constructed from measurements of the i -th parameter X_i using

$$\gamma_v(\tau) = \frac{1}{2}E \left[(X_i(\mathbf{x}_1) - X_i(\mathbf{x}_2))^2 \right], \quad \forall \|\mathbf{x}_1 - \mathbf{x}_2\| = \tau \quad (8)$$

where τ is the spatial distance between two points and E is the expected value operator (mean). For spatially limited correlation, $\lim_{\tau \rightarrow \infty} \gamma_v(\tau)$ represents the variance of the random field:

$$\lim_{\tau \rightarrow \infty} \gamma_v(\tau) = \text{var}[\varepsilon_t] \quad (9)$$

In the geomechanical literature, it is more common to express the semi-variogram in the normalised form using the autocorrelation coefficient $\rho(\tau)$ (in this graph it is denoted as a *correlogram*), which, for zero experimental uncertainty $\text{var}[\varepsilon_e] = 0$, reads

$$\rho(\tau) = 1 - \frac{\gamma_v(\tau)}{\text{var}[\varepsilon_t]} \quad (10)$$

The correlogram may be modelled in different ways; in geomechanical literature the Markov exponential model is popular (Vanmarcke (1983), Griffiths & Fenton (2004)):

$$\rho(\tau) = \exp\left(\frac{-2\tau}{\theta}\right) \quad (11)$$

with the parameter θ denoted as the correlation length. Both the semi-variogram (normalised by $\text{var}[\varepsilon_t]$) and correlogram for zero experimental uncertainty $\text{var}[\varepsilon_e] = 0$ are shown in Fig. 1.

Quantification of spatial correlation properties for non-zero experimental uncertainty

Spatial correlation properties for non-zero experimental uncertainty can be expressed using a total semi-variogram (Smith, 2014), which includes both the natural spatial variability and the experimental uncertainty. Such a semi-variogram is depicted in Fig. 2, together with three characteristics denoted in statistics as "nugget", "range" and "sill". They are equivalent to $\text{var}[\varepsilon_e]$, correlation

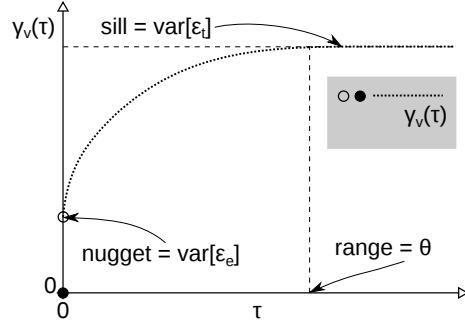


Figure 2: Total semi-variogram for non-zero experimental uncertainty.

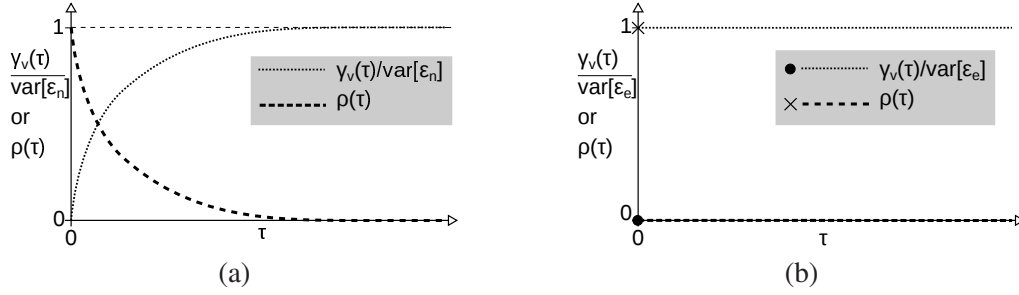


Figure 3: (a) Normalised semi-variogram and correlogram for natural spatial variability, (b) discontinuous normalised semi-variogram and correlogram for experimental uncertainty.

length θ and $\text{var}[\epsilon_t]$, respectively, using the terminology adopted in this paper.

For the purpose of introducing the spatial statistical analysis into a code with non-zero element size, however, the developments are not based on the total semi-variogram from Fig. 2. Instead, separate variograms (or correlograms) are considered for natural variability and for experimental uncertainty. The semi-variogram for natural variability is formally the same as the semi-variogram introduced in the previous subsection (Fig. 1), normalised with respect to $\text{var}[\epsilon_n]$ instead of $\text{var}[\epsilon_t]$. $\text{var}[\epsilon_n]$ is calculated using Eq. (7). This semi-variogram is shown in Fig. 3a. The semi-variogram for the experimental uncertainty is different; since the experimental uncertainty is assumed to be spatially independent (Eq. (3)), its semi-variogram and correlogram are discontinuous (Fig. 3b), with perfect correlation for $\tau = 0$ and zero correlation for $\tau > 0$.

Spatial correlation for analysis with elements of finite size

When random field analysis is incorporated into the finite element method (or any other method with non-zero size of calculation units, denoted as elements in finite element and difference methods), the following problem must be considered. Spatial characteristics described in the previous sections are relevant for calculation units of infinitesimal size. For elements of finite size, the

variability of parameters (measured by their variance) must be reduced, due to the averaging of property values *within* the finite element. This spatial averaging of soil properties over the finite element is denoted as *local averaging* (Vanmarcke, 1983). The variance reduction factor γ is for zero experimental uncertainty calculated as:

$$\text{var}[\varepsilon_t]_A = \gamma \text{var}[\varepsilon_t] \quad (12)$$

where $\text{var}[\varepsilon_t]_A$ is the variance of the spatially-averaged random field which enters the random field simulations instead of $\text{var}[\varepsilon_t]$. The variance reduction factor γ is for the correlogram described using Eq. (11) and for a 2D square finite element calculated by integration of (11) as (Vanmarcke, 1983):

$$\gamma = \frac{4}{(\alpha\theta)^4} \int_0^{\alpha\theta} \int_0^{\alpha\theta} \exp\left(-\frac{2}{\theta}\sqrt{x^2 + y^2}\right) (\alpha\theta - x)(\alpha\theta - y) dx dy \quad (13)$$

where x, y are local spatial coordinates within the element frame of reference, θ is the correlation length and $\alpha = a/\theta$ is the element size factor, with a being the size of the square finite element.

For the random field simulations with non-zero experimental uncertainty, the separate semi-variograms shown in Fig. 3 are used. The variance reduction factor γ_n for spatial variability is calculated using Eq. (13). Spatial variability is then introduced by reducing the variance $\text{var}[\varepsilon_n]$ calculated using (7) instead of reducing $\text{var}[\varepsilon_t]$ as is done in "standard" random field simulations, which neglect the experimental uncertainty. Thus,

$$\text{var}[\varepsilon_n]_A = \gamma_n \text{var}[\varepsilon_n] = \gamma_n (\text{var}[\varepsilon_t] - \text{var}[\varepsilon_e]) \quad (14)$$

The variance reduction factor for the experimental variability γ_e comes from the integration of the discontinuous correlogram from Fig. (3b). It follows that for the non-zero element size γ_e is equal to 0. That is, experimental variability enters the random field simulations only through the quantification of $\text{var}[\varepsilon_n]$ from the known $\text{var}[\varepsilon_t]$ and $\text{var}[\varepsilon_e]$. Since the variance reduction factor γ_n is the same in the analyses neglecting and considering the experimental uncertainty, the incorporation of the experimental uncertainty into random field simulations requires no adjustments of the existing software. The total parameter variance $\text{var}[\varepsilon_t]$ must only be replaced by $\text{var}[\varepsilon_n]$.

Implications of neglecting the experimental variability

The above analysis implies a possibly counter-intuitive effect of experimental variability. The increase of experimental uncertainty *for the given total variability* measured in the spatial grid using non-perfect experimental methods *decreases* the parameter variance that should enter random field simulations. Consequently, it also reduces the variance of the performance function. Statistics of

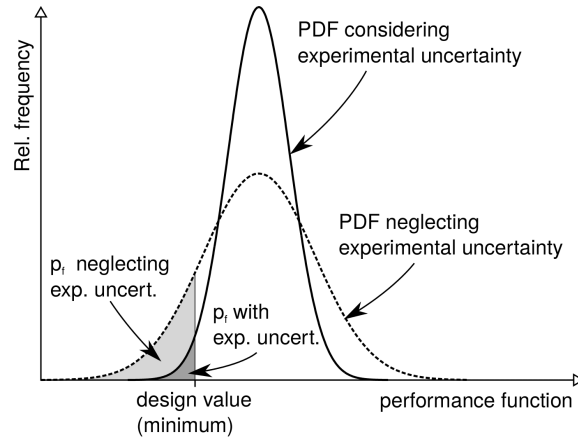


Figure 4: Sketch of the influence of experimental uncertainty on the calculated probability of unsatisfactory performance p_f (sketched for the case when the performance is unsatisfactory for the performance function lower than the design value, applicable for example for factor of safety).

the performance function may be used to quantify the *probability of unsatisfactory performance* p_f (Duncan, 2000). It represents the area under the probability density function (PDF) for calculated values that are lower than the limiting design value (in the case when the design value is the minimum, for example factor of safety), or it represents the area under the PDF for calculated values that are higher than the limiting design value (in the case when the design value is the maximum, for example foundation settlement or lining bending moment). The effect of experimental variability is demonstrated in Fig. 4. It follows that for $p_f < 50\%$ consideration of experimental uncertainty *decreases* the probability of unsatisfactory performance. A specific example is given later in this paper.

Experience shows that probabilistic methods in geotechnical engineering overpredict the probability of unsatisfactory performance. For example, Griffiths & Fenton (2004) noted that, for the case they studied, a direct conversion of the factor of safety $FS = 1.47$ into the probability of slope failure without considering spatial variability yielded $p_f = 28\%$, a remarkably high value considering that slopes with $FS = 1.47$ rarely fail. It is now well established that this discrepancy may be explained by means of spatial averaging (Griffiths & Fenton, 2004). In this paper, it is argued that overprediction of the probability of unsatisfactory performance may additionally be caused by neglecting the experimental variability in random field simulations.

Incorporation of sampling uncertainty

At this point, let us continue our analysis by considering the *sampling uncertainty*, which is the uncertainty derived from the fact that the total and experimental uncertainties have been evaluated

using an insufficient number of samples.

Quantification of sampling uncertainty

All the directly measured statistical characteristics involved in the simulations are subject to sampling uncertainty, that is $\mu[X_i]$, $\text{var}[\varepsilon_t[X_i](\mathbf{x})]$ and $\text{var}[\varepsilon_e[X_i]]$ (abbreviated as μ , $\text{var}[\varepsilon_t]$ and $\text{var}[\varepsilon_e]$). In this section, these quantities become random variables. For clarity, their values obtained by evaluation (of a finite number) of experiments are distinguished using a circumflex accent $\hat{\sigma}$.

In the following, n_t denotes the number of samples used in the evaluation of the spatial variability and n_e is the number of samples used in the evaluation of the experimental uncertainty. For normally distributed parameters (Hald (1951), Booy & Lye (1989))

$$\sigma_s[\hat{\mu}] = \frac{\hat{\sigma}[\varepsilon_t]}{\sqrt{n_t}} \quad (15)$$

$$\sigma_s^2[\hat{\sigma}^2[\varepsilon_t]] = \frac{2\hat{\sigma}^4[\varepsilon_t]}{n_t - 1} \quad (16)$$

$$\sigma_s^2[\hat{\sigma}^2[\varepsilon_e]] = \frac{2\hat{\sigma}^4[\varepsilon_e]}{n_e - 1} \quad (17)$$

where the subscript $_s$ is adopted to indicate sampling uncertainty. Note that Eqs. (15) to (17) are approximate only, as the sampling uncertainty should be calculated from the exact values of $\sigma[\varepsilon_t]$ and $\sigma[\varepsilon_e]$ (not from their experimental estimates $\hat{\sigma}[\varepsilon_t]$ and $\hat{\sigma}[\varepsilon_e]$). Also, they are valid for non-correlated variables only (this is satisfied for experimental uncertainty, but not for total uncertainty with distance-dependent autocorrelation coefficient ρ).

To incorporate the sampling uncertainty into the random field simulations with a calculation unit of finite size, the sampling standard deviation of $\hat{\sigma}[\varepsilon_n]$ (denoted as $\sigma_s[\hat{\sigma}[\varepsilon_n]]$) must be quantified. It follows from the rules of statistics that for two uncorrelated normally distributed variables X and Y

$$\text{var}[X - Y] = \text{var}[X] + \text{var}[Y] \quad (18)$$

Therefore, from (16) and (17):

$$\sigma_s^2[\hat{\sigma}^2[\varepsilon_n]] = \frac{2\hat{\sigma}^4[\varepsilon_t]}{n_t - 1} + \frac{2\hat{\sigma}^4[\varepsilon_e]}{n_e - 1} \quad (19)$$

At this point, the following rule of statistics is employed:

$$\sigma^2[X^2] = 2\sigma^2[X] (\sigma^2[X] + 2\mu^2[X]) \quad (20)$$

to quantify $\sigma_s [\hat{\sigma}[\varepsilon_n]]$. A quadratic equation is obtained with two roots: one negative and one positive. As standard deviation must be positive, the equations yield a single valid solution, which after algebraic manipulations reads:

$$\sigma_s [\hat{\sigma}[\varepsilon_n]] = \sqrt{-\hat{\sigma}^2[\varepsilon_n] + \sqrt{\hat{\sigma}^4[\varepsilon_n] + \frac{\sigma_s^2 [\hat{\sigma}^2[\varepsilon_n]]}{2}}} \quad (21)$$

where $\sigma_s^2 [\hat{\sigma}^2[\varepsilon_n]]$ is given by (19).

Incorporation of sampling uncertainty into the random field method

The most general approach for quantifying sampling uncertainty within a random field method is the *two-dimensional Monte-Carlo simulation* (Hofer *et al.*, 2002). In this method a nested Monte-Carlo simulation is run for each of the random field realisations, keeping the same random field structure (the random field is defined by means of normalised random variables, which do not change within the nested Monte-Carlo run). $\mu[X_i]$ and $\sigma[\varepsilon_n[X_i]]$ in the nested Monte-Carlo loop are considered as random variables with mean values $\hat{\mu}[X_i]$ and $\hat{\sigma}[\varepsilon_n[X_i]]$ and standard deviations $\sigma_s [\hat{\mu}[X_i]]$ (Eq. (15)) and $\sigma_s [\hat{\sigma}[\varepsilon_n[X_i]]]$ (Eq. (21)), respectively. Formally, $2n$ random variables are thus involved in the nested Monte-Carlo loop (n is the number of parameters).

The two-dimensional Monte-Carlo simulation is computationally extremely demanding. To simplify it, let us formally describe the computational model as

$$Y = g(X_1, X_2, \dots, X_n) \quad (22)$$

where Y is the performance function (simulation result, such as the factor of safety). In the simplified analysis, the mean value and variance of Y due to natural variability considering the effect of experimental uncertainty (denoted as $\mu_n[Y]$ and $\text{var}_n[Y]$) may be found using random field analysis with parameter statistics $\hat{\mu}[X_i]$ and $\hat{\sigma}[\varepsilon_n[X_i]]$. Next, a single random field realisation is selected (preferably the one leading to $Y \sim \mu_n[Y]$) and a single Monte-Carlo simulation is run with a fixed random field structure that has variable $\mu[X_i]$ and $\sigma[\varepsilon_n[X_i]]$ using their mean values $\hat{\mu}[X_i]$ and $\hat{\sigma}[\varepsilon_n[X_i]]$ and standard deviations $\sigma_s [\hat{\sigma}[\varepsilon_n[X_i]]]$ (Eq. (21)) and $\sigma_s [\hat{\mu}[X_i]]$ (Eq. (15)) leading to the performance function statistics $\mu_s[Y]$ and $\text{var}_s[Y]$. The assumption of statistical independence of sampling uncertainty and natural variability then yields

$$\text{var}[Y] = \text{var}_n[Y] + \text{var}_s[Y] \quad (23)$$

$$\mu[Y] = \mu_n[Y] \quad (24)$$

To further simplify the simulations, it is pointed out that the Monte-Carlo run for sampling uncertainty does not involve variation of the random field structure. It may thus be quite reliably substituted by simpler probabilistic methods such as the first order second moment (FOSM) method or one of the point estimate methods (Christian & Baecher (1999), Rosenblueth (1981), Zhou & Nowak (1988)). When expressed using the FOSM method, the value of $\text{var}_s[Y]$ reads

$$\text{var}_s[Y] = \frac{1}{4} \sum_{j=1}^{n_{FOSM}} [g(\mu[R_j] + \sigma[R_j]) - g(\mu[R_j] - \sigma[R_j])]^2 \quad (25)$$

where R_j formally denotes the uncertain variables ($\mu[X_i]$ and $\sigma[\varepsilon_n[X_i]]$). It follows that $n_{FOSM} = 2n$ (standard deviation and mean of each parameter X_i is involved as an uncertain variable). The FOSM method therefore requires $4n$ runs of the performance function, a comparatively lower number than the potentially thousands of runs required by the Monte-Carlo method.

Geotechnical engineering example

In this section, an example of application of the proposed approach is given. The underlying case has been thoroughly described in Suchomel & Mašín (2011). They studied the total variability of a sandy soil using experiments on samples obtained from a regular grid in a quarry wall. The results have been used in simulations of a strip footing settlement using a hypoplastic model. In this paper, an additional experimental data set is presented quantifying the experimental uncertainty and its effect is evaluated using random field simulations.

Experimental data quantifying natural variability

The soil studied comes from the upper Cretaceous basin in south Bohemia (Czech Republic). The sediments of the basin are fluvial, characterised by a variation of gravely sands, sands and clayey sands. As these materials can all be modelled using a single constitutive model (hypoplastic model has been selected), where the variation in granulometry is represented by the parameter variability, the case study is suitable for utilisation of probabilistic methods based on random fields. For material model calibration, thirty-seven samples for testing total variability were extracted from the quarry wall in a grid depicted in Fig. 5 (three out of forty samples shown in Fig. 5 could not be used in the analyses due to experimental problems). It is to be pointed out that the samples extracted from the quarry wall have been disturbed; we have thus focused on quantification of variability due to soil composition reflected by the hypoplastic model parameters, not on possible variability of *in-situ* void ratio. The testing programme consisted of the following experiments:

1. Angle of repose test
2. Oedometric test. The oedometric specimens were prepared by air pluviation of the dry sand without any compaction and subsequent flooding. The aim was to prepare specimens of minimum relative density which are most suitable for asymptotic state quantification (Mašín, 2012).
3. Triaxial test. The triaxial specimens were prepared by a spooning of saturated samples directly into the triaxial mold of the diameter of 38 mm, using the procedure described in Tatsuoka *et al.* (1979) and Wichtmann & Triantafyllidis (2012). As noted by Head (1985), saturated spooning is preferable to placing the sample dry and subsequent flooding, as it is difficult to ensure full saturation in the latter case. The sample has been prepared to the total height of 78 mm in five layers, with each layer having been thoroughly densified by tamping (Tatsuoka *et al.*, 1979) using rod of 20 mm in diameter. As the parameters of the hypoplastic model depend on granulometry only and not on relative density (Herle & Gudehus (1999), Hájek *et al.* (2009)), the tamping energy has not been controlled precisely; instead, approximately the same tamping energy has been applied on all the samples by the experimentalist. After the sample preparation, it has been consolidated isotropically up to the effective stress of 200 kPa (under a backpressure of 200 kPa) and sheared drained up to failure.

Figure 6a shows summary of the all angle of repose test results, Figures 7a and 8a give a summary of the triaxial test results and Figure 9a shows all the oedometric curves. Summary graphs are presented only for brevity, without any indication of location of the individual samples within the sampling grid; for detailed information, the readers are referred to Suchomel & Mašín (2011). Note that the sample preparation method probably contributed to the variations in the initial void ratio; however, it should not have a major influence on the calibration results, as the initial void ratio does not affect substantially the hypoplastic model parameters.

Suchomel & Mašín (2011) used the experimental results to calibrate the hypoplastic model given by von Wolffersdorff (1996). The model requires eight parameters: φ_c , h_s , n , e_{c0} , e_{d0} , e_{i0} , α and β . A detailed description of the model parameters and their calibration procedures can be found in von Wolffersdorff (1996) and Herle & Gudehus (1999); here we present their summary only for brevity:

- φ_c is the critical state friction angle.
- Parameters h_s , n , e_{c0} , e_{d0} and e_{i0} define the limiting void ratio lines, prescribed by Bauer (1996)

$$e = e_{p0} \exp \left[- \left(\frac{3p}{h_s} \right)^n \right] \quad (26)$$

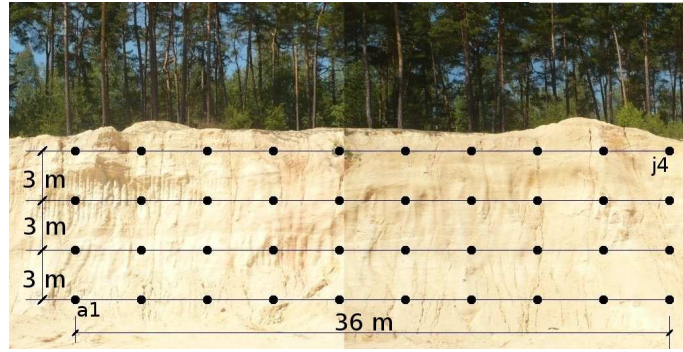


Figure 5: The wall of the sand pit indicating positions of specimens for investigation of total variability (from Suchomel and Mašín 2011). Note that three samples e4, f1 and f2 could not be tested successfully.

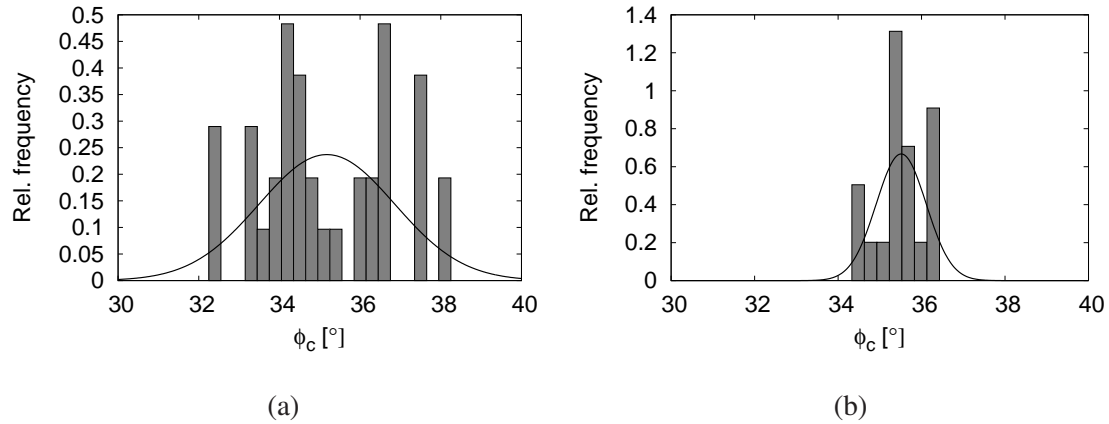


Figure 6: Normalised histograms and Gaussian fits for the angle of repose test. (a) experiments on total variability, (b) experiments on experimental uncertainty.

where p is the mean effective stress and e_{p0} is substituted by e_{d0} for the minimum void ratio, e_{c0} for the critical state void ratio and e_{i0} for the theoretical state of minimum relative density.

- Parameter α controls the dependency of peak friction angle on relative density (increase of α increases the peak friction angle for the given relative density). The model automatically predicts an increase of peak friction angle with increasing relative density.
- Parameter β controls the dependency of soil stiffness on relative density and mean effective stress (increase of β increases stiffness for the given relative density and mean effective stress). The model automatically predicts an increase of soil stiffness with increasing relative density and with increasing stress.

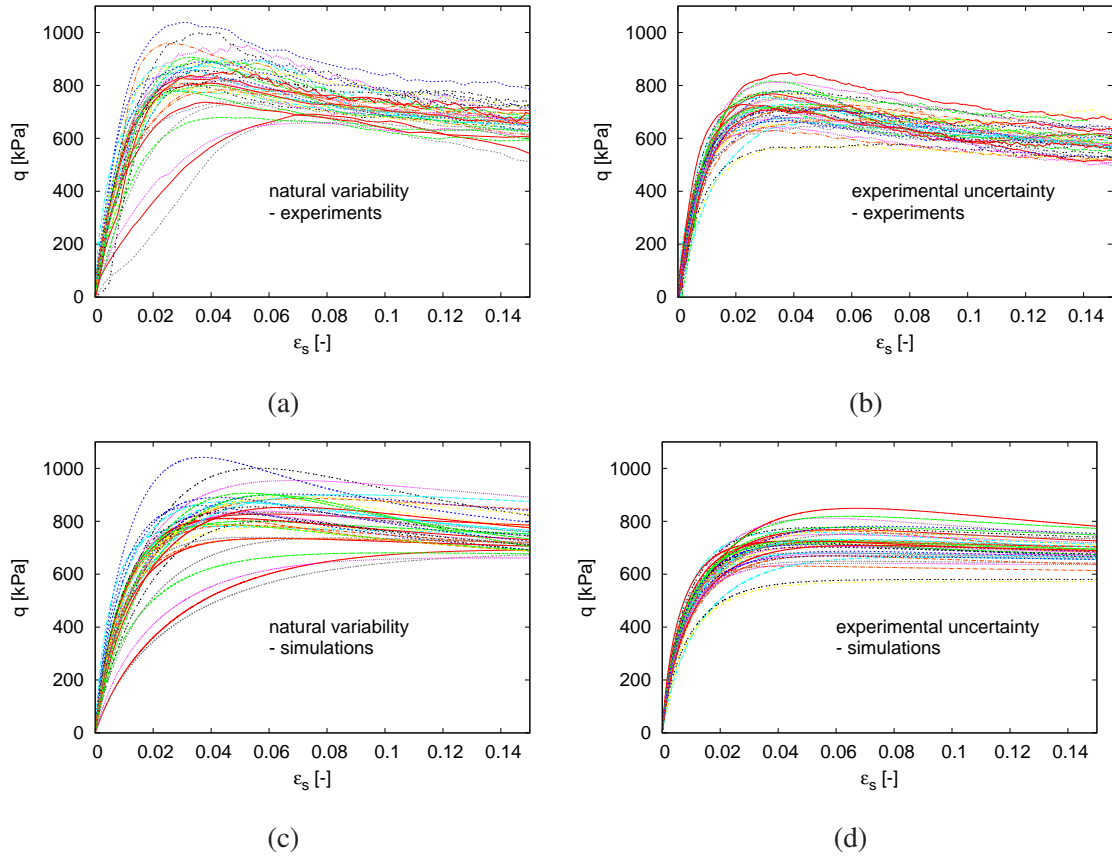


Figure 7: Stress-strain curves of drained triaxial tests. Experimental curves of the tests on total variability (a) and experimental uncertainty (b); simulated curves of the tests on total variability (c) and experimental uncertainty (d).

The parameters were calibrated as follows. φ_c was measured directly using the angle of repose test (Figure 7a). h_s , n and e_{c0} were calibrated using the oedometric tests, such that they can be represented using equation (26) where $e_{p0} \approx e_{c0}$ was assumed. The mean effective stress p has been calculated from the vertical stress σ_v using the formula by Jáký (1944) leading to $p = \sigma_v(1 - 2 \sin \varphi_c/3)$. e_{d0} and e_{i0} were estimated from e_{c0} using the empirical correlations $e_{d0} = 0.38e_{c0}$, $e_{i0} = 1.2e_{c0}$ (Suchomel & Mašín, 2011). The parameters α and β were calibrated using the triaxial test results. α was calibrated so that the model represented the exact peak friction angle and β was calibrated to predict the shear stiffness at $q = 0.5q_{max}$, where q_{max} is the peak deviator stress. All the parameters were calibrated using automated scripts to limit ambiguity of calibration. Note that the oedometric experiments conducted by Suchomel & Mašín (2011) were performed up to vertical stresses of 6400 kPa, whereas the new data set on experimental uncertainty was performed up to 3200 kPa. For consistency, the model was re-calibrated (loading step 3200 kPa to 6400 kPa was not considered) and the parameters thus differ slightly from those presented in Suchomel & Mašín (2011).

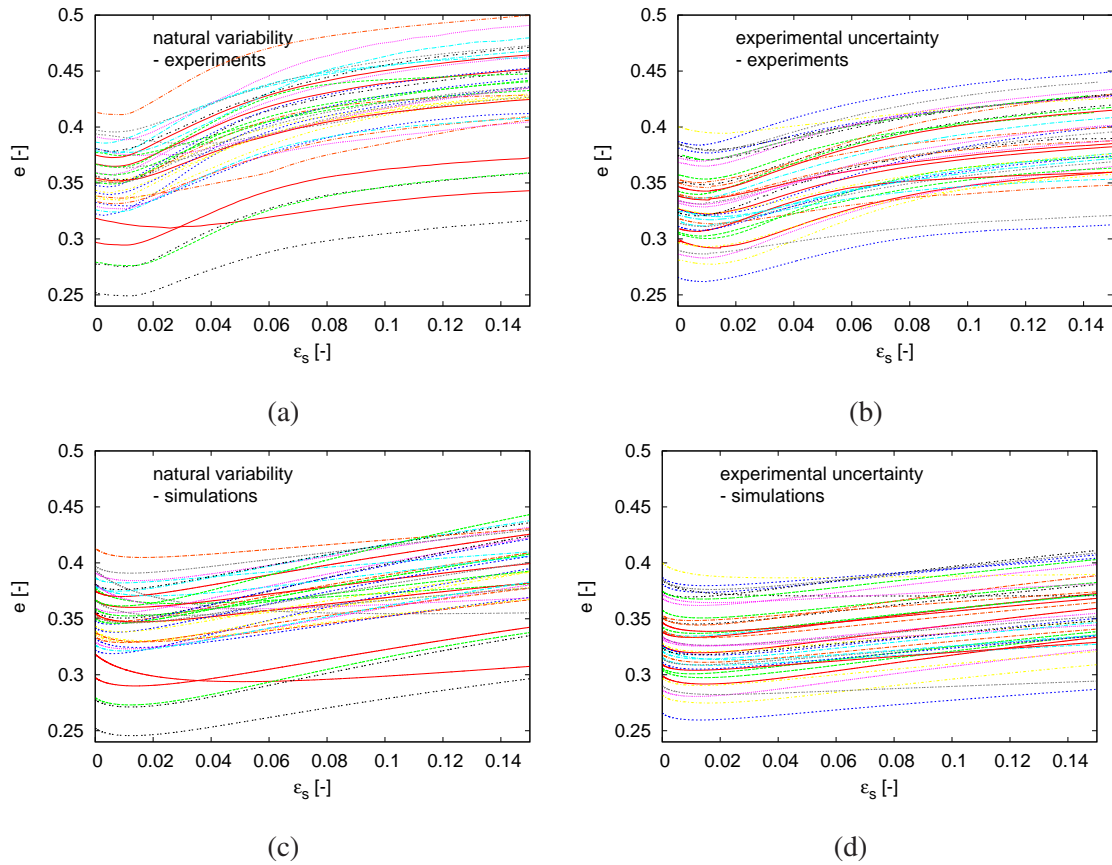


Figure 8: Void ratio variation curves from drained triaxial tests. Experimental curves of the tests on total variability (a) and experimental uncertainty (b); simulated curves of the tests on total variability (c) and experimental uncertainty (d).

Figures 7c, 8c and 9c show the simulations of the laboratory experiments with the obtained parameter sets, indicating a reasonably good fit. The oedometric curves (Figure 9) have been obtained by directly plotting Eq. (26), whereas the triaxial curves (Figure 7) have been obtained by single element simulations of the experiments using the hypoplastic model. Histograms of the parameters with Gaussian fits are shown in Fig. 10a (logarithms of parameter values approximated in the case of log-normally distributed parameters); the parameters of the distributions are in Table 1. Some parameters were more closely approximated by a log-normal distribution and some by the Gaussian distribution. The more suitable distribution was selected using the Kolmogorov-Smirnov test.

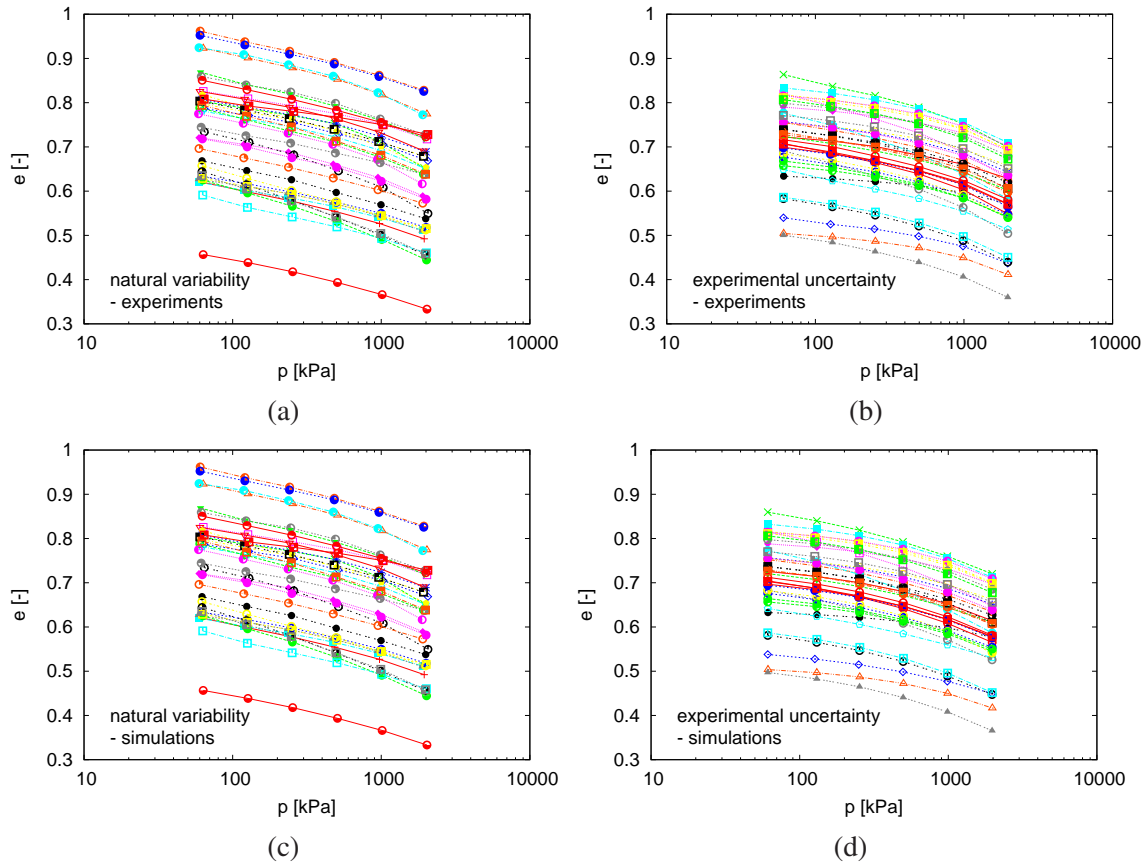


Figure 9: Oedometric test results. Experimental curves of the tests on total variability (a) and experimental uncertainty (b); simulated curves of the tests on total variability (c) and experimental uncertainty (d).

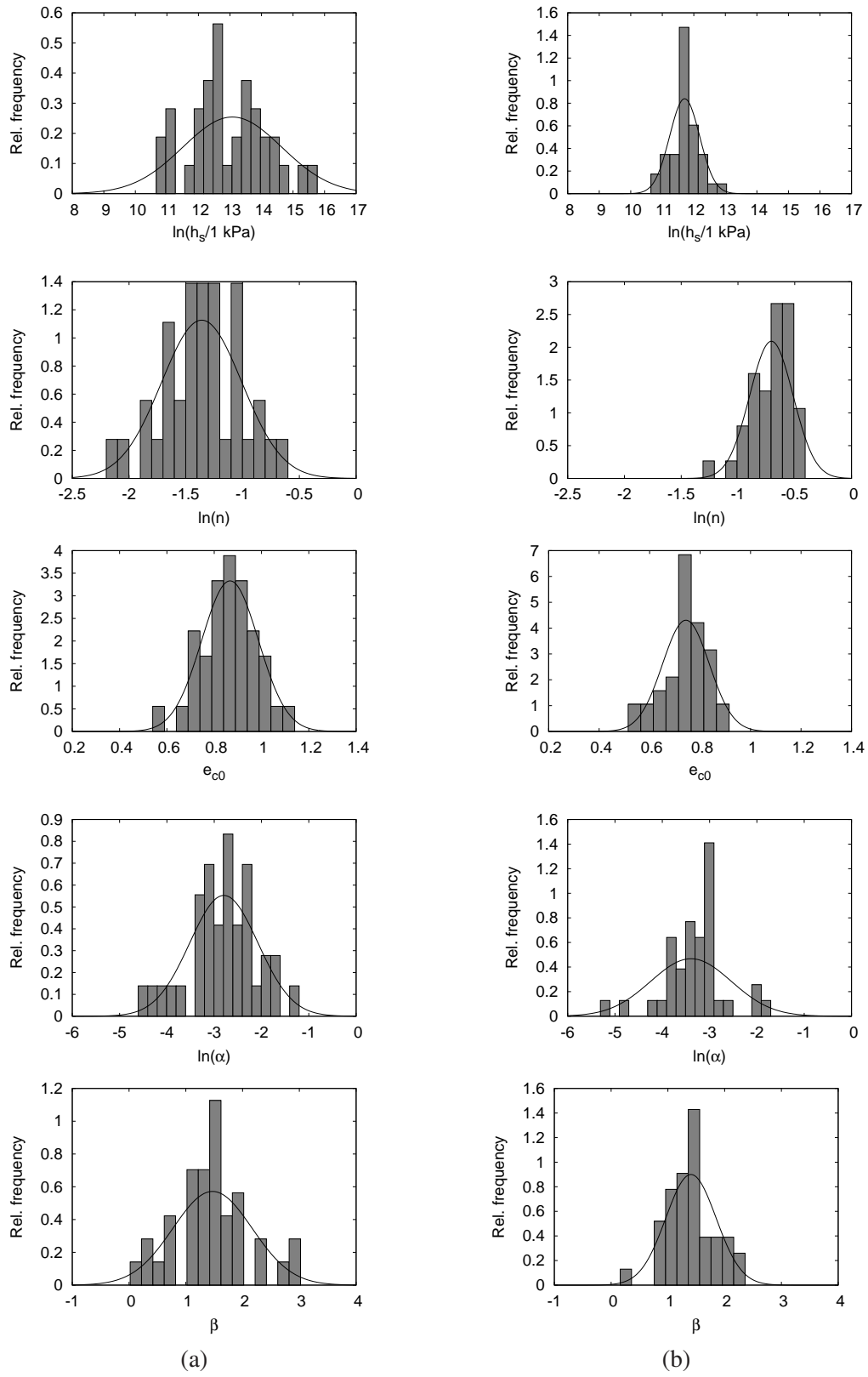


Figure 10: Normalised histograms and Gaussian fits of hypoplastic model parameters. (a) total variability, (b) experimental uncertainty.

Table 1: Characteristic values of statistical distributions of the hypoplastic model parameters (values in *italics* were obtained from empirical correlations rather than direct calibration).

parameter	total		experimental		ratio
	mean	st. dev.	mean	st. dev.	$\text{var}[\varepsilon_e]/\text{var}[\varepsilon_t]$
$\varphi_c[^\circ]$	35.177	1.683	35.513	0.597	0.126
$\ln(h_s/1\text{kPa})$	13.075	1.569	11.709	0.475	0.092
$\ln n$	-1.360	0.354	-0.706	0.191	0.290
e_{c0}	0.867	0.120	0.744	0.093	0.598
e_{i0}	<i>1.041</i>	<i>0.144</i>	<i>0.893</i>	<i>0.111</i>	<i>0.598</i>
e_{d0}	<i>0.328</i>	<i>0.045</i>	<i>0.281</i>	<i>0.035</i>	<i>0.598</i>
$\ln \alpha$	-2.796	0.722	-3.393	0.853	1.397
β	1.471	0.698	1.406	0.443	0.403

Suchomel & Mašín (2011) also evaluated the correlation length using the φ_c measurements. The correlogram was represented by the Markov function (11) enhanced by considering different correlation lengths in the horizontal (θ_h) and vertical (θ_v) directions, which led to $\theta_h = 242$ m and $\theta_v = 5.1$ m. However, the estimation of horizontal correlation length was very approximate due to insufficient data in the lateral plane (Uzielli *et al.* (2005), DeGroot & Baecher (1993)), and the vertical correlation length estimation was also not reliable, as the vertical sampling distance of 3 m was too high to reveal the vertical scale of fluctuation. For a more accurate estimation of vertical correlation length, additional angle of repose tests were performed using 100 samples obtained from a 5m high profile with 0.05m vertical sampling distance, which led to a more precise estimation of $\theta_v = 0.31$ m. Suchomel & Mašín (2011) subsequently conducted a numerical parametric study on the influence of correlation length on the simulation results.

In this work, the investigation of the correlation length effect is not a scope of the paper; instead, we aim to demonstrate the effect of experimental and sampling uncertainties. As considering the low correlation length of $\theta_v = 0.31$ m requires very fine finite element meshes and computationally demanding simulations, we performed the simulations using fixed values of $\theta_h = 242$ m and $\theta_v = 5.1$ m, noting that for the present case study the adopted value of θ_v is unrealistically high. The selection of θ_v would affect the standard deviations of the performance function and thus also the calculated probability of unsatisfactory performance, but not the qualitative effect of the experimental and sampling uncertainties on the simulation results.

Experimental data quantifying experimental uncertainty

A new set of experiments was performed to quantify the experimental uncertainty (Mayer, 2013). This experimental programme was identical to that used to evaluate total variability; however, soil was obtained from a single location within the quarry wall². The experiments were performed on forty nominally identical samples, which were prepared from the main sample using the cone and quartering method. The main sample of approx. 10 kg has first been mixed thoroughly. The technique then involved pouring the sample into a cone, flattening the cone, dividing the flattened cone into four equal divisions (quartering), removing two opposite quarters and repiling the other two into a new cone (Schumacher *et al.*, 1990).

The experiments were performed in the same soil mechanics laboratory using the same triaxial and oedometric apparatus as the experiments aimed at quantification of the spatial variability. The two experimental data sets have been performed by two different experimentalists; however, one experimentalist performed all the tests within one experimental data set. The preparation procedure for the individual samples was identical to the preparation of the samples for testing spatial variability.

Figure 6b shows results of the angle of repose tests, Figures 7b and 8b summarise the triaxial test results and Figure 9b shows all the oedometric curves. The results show a substantial scatter, in particular in the peak strength measured in the triaxial test and in the initial void ratio of both the oedometric and triaxial tests. Visual comparison with the tests on total variability (Figs. 7a, 8a and 9a), however, reveals that these experimental results are even more variable. Figures 7d, 8d and 9d show simulations of the experiments using the hypoplastic model. A reasonably good approximation is obtained, indicating that the statistics of the model parameters may be considered as representative for the uncertainty evaluation. Histograms of the hypoplastic model parameters with Gaussian fits are shown in Fig. 10b (log-transformed parameters were fit in the case of log-normally distributed parameters), and the parameters of the distributions are given in Tab. 1.

Tab. 1 also gives the ratios of parameter variances of data sets on total variability and experimental uncertainty. Lower values of this ratio (indicating relatively low experimental variability) apply to the angle of repose (φ_c) and parameters controlling the slope of the oedometric curve (h_s and n). In contrast, higher values were obtained for the initial void ratio measurements (e_{c0}) and for parameters controlling the triaxial stress-strain curves α and β . In fact, $\text{var}[\varepsilon_e]/\text{var}[\varepsilon_t]$ for the parameter α is higher than one, which is theoretically not possible and other effects not considered in this paper probably play a role here (for example uncertainty in the model calibration, different sampling location for the tests on experimental uncertainty, etc).

²Note that due to the quarry wall advance between the sample collection, the new sample could not be extracted exactly from the section shown in Fig. 5. It was, however, ensured the new sample had a geologically equivalent position to the samples obtained earlier.

Description of the finite element model

The influence of the experimental and sampling uncertainties was investigated by the random field simulation of the settlement of a strip footing. The simulated problem aimed to demonstrate the concept and did not correspond to any real case study. The problem characteristics were taken from Suchomel & Mašín (2011). Simulations were performed using a finite element package *Tochnog Professional* (Rodemann, 2008). The problem geometry and the finite element mesh are shown in Figure 11. The mesh consisted of 1920 nine-noded quadrilateral elements. The foundation was analysed as rigid and perfectly smooth. The soil unit weight was 18.7 kN/m^3 . The initial earth pressure coefficient at rest was $K_0 = 0.43$ (calculated from the Jáký (1944) formula using an average value of φ_c). The initial void ratio $e = 0.48$ was used in the simulations.

The random fields of the input variables were generated using a Cholesky decomposition of the correlation matrix (e.g., Fenton (1997)). All the parameters have been considered as uncorrelated, with the exception of e_{c0} , e_{d0} and e_{i0} , which were perfectly correlated (this is because e_{d0} and e_{i0} were calculated from e_{c0} using an empirical relationship). Cross-correlation between the individual parameters has been investigated, with statistically significant cross-correlation only being observed between the parameters α and β ($R^2 = 0.6$), α and e_{c0} ($R^2 = -0.71$) and α and φ_c ($R^2 = -0.51$) (the cross-correlation matrix is presented in Suchomel & Mašín (2011)). However, the effect of parameter correlation has not been studied within this paper and the correlations have thus been neglected.

In the simulations, foundation displacements u_y corresponding to the load of 100 kPa were evaluated. The probability of unsatisfactory performance was calculated with respect to foundation settlements of 0.09 m.

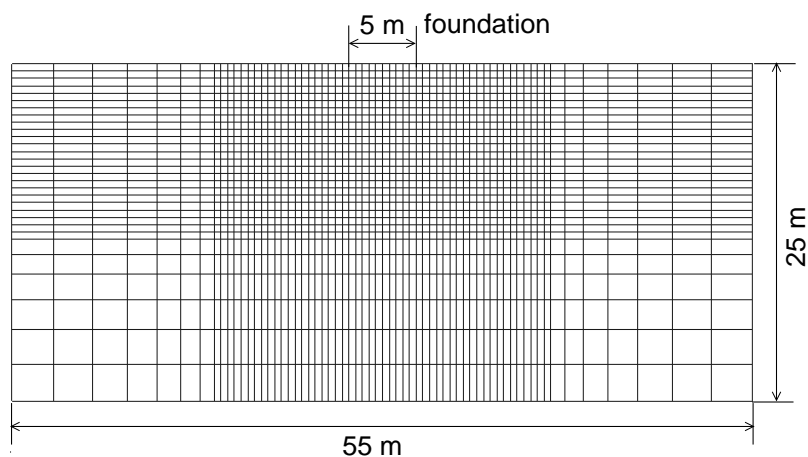


Figure 11: Finite element mesh.

The influence of experimental uncertainty on the probability of unsatisfactory performance

The influence of experimental uncertainty was included using Eq. (14). The Monte-Carlo method was used to quantify the statistics of the performance function. To ensure the accuracy of the simulations the number of realisations was always larger than 5000; this is significantly higher than the minimum number of realisations (700) identified by Suchomel & Mašín (2011)). The simulations were run for the total variability and experimental uncertainty obtained from the experiments. In addition, the influence of experimental uncertainty was further studied by varying it using a multiplier m_e such that

$$\text{var}[\varepsilon_n]_A = \gamma_n \text{var}[\varepsilon_n] = \gamma_n \langle \text{var}[\varepsilon_t] - m_e \text{var}[\varepsilon_e] \rangle \quad (27)$$

The value of $m_e = 0$ thus signifies a "standard" random finite element simulation, which does not consider the effect of experimental uncertainty. The value of $m_e = 1$ implies parameter statistics obtained from the present experiments. $0 < m_e < 1$ means experimental uncertainty lower than observed in the present experiments and $m_e > 1$ means experimental uncertainty higher than observed in the present experiments. $\text{var}[\varepsilon_n]$ equal to zero was assumed for negative values of $(\text{var}[\varepsilon_t] - m_e \text{var}[\varepsilon_e])$ (the Macaulay bracket $\langle x \rangle$ in Eq. (27) gives a positive part of x , i.e. $\langle x \rangle = (x + |x|)/2$).

Fig. 12 shows the random fields of the parameters h_s , n and β for one of the Monte-Carlo realisations with $m_e = 1$, which yielded u_y very close to the median value of u_y obtained in the complete Monte-Carlo run. Suchomel & Mašín (2011) have shown, using sensitivity analysis, that h_s , n and β were the most influential parameters in these simulations.

The value of the foundation vertical displacement closely matched a log-normal distribution. An example simulation outcome showing the log-transformed value of u_y for $m_e = 1$ and its Gaussian fit is shown in Fig. 13.

Figure 14a shows how the mean value and standard deviation of Gaussian distributions fitted to $\ln(u_y/1m)$ are dependent on m_e . While the experimental uncertainty has only a minor effect on the mean value of $\ln(u_y/1m)$, the standard deviation of the performance function is significantly influenced. An increase in the experimental uncertainty (increase of m_e) for the *given* total variability decreases the standard deviation of $\ln(u_y/1m)$. As explained earlier (recall Fig. 4), the experimental uncertainty affects the probability of unsatisfactory performance. Its value for natural variability and experimental uncertainty (denoted as p_n) for different values of m_e is depicted in Fig. 14b. For the simulated problem, "standard" random field simulations ignoring experimental uncertainty ($m_e = 0$) yielded $p_n = 13.9\%$ and simulations that considered experimental uncertainty with the current parameter set ($m_e = 1$) yielded $p_n = 10.5\%$. Thus, with increasing m_e , the

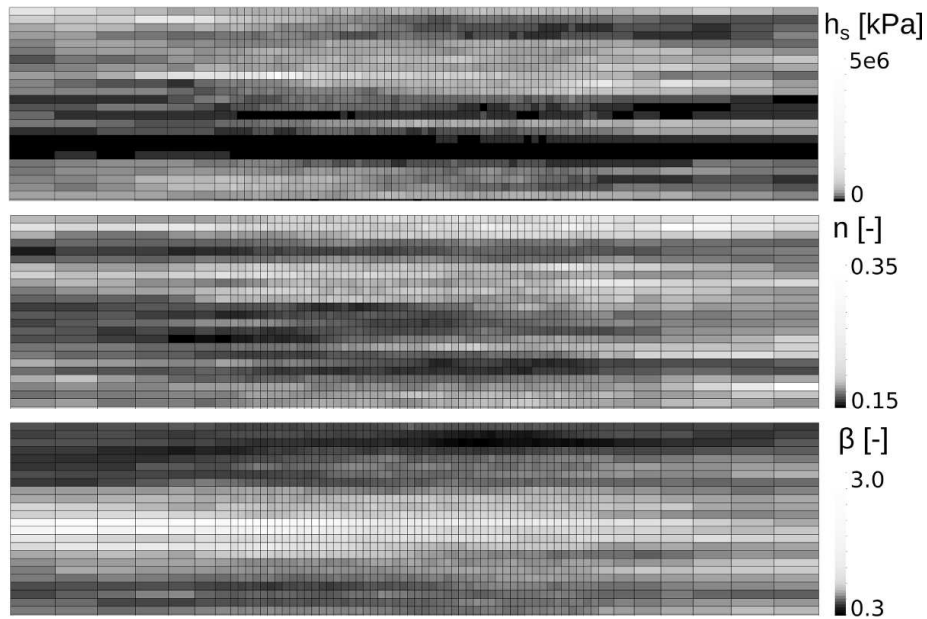


Figure 12: Random fields of natural variability ($m_e = 1$) of the most influential parameters h_s , n and β for one of the Monte-Carlo realisations. The bottom part of the mesh is not shown.

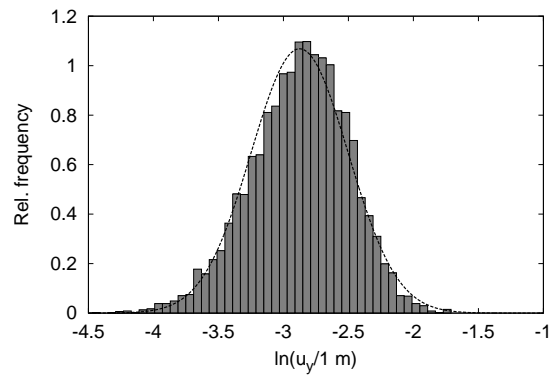


Figure 13: Histogram and log-normal fit of u_y obtained in the Monte-Carlo simulation ($m_e = 1$, 8000 realisations).

probability of unsatisfactory performance decreases to zero.

The influence of sampling uncertainty on the probability of unsatisfactory performance

To study the influence of sampling uncertainty the FOSM method was adopted, which was first evaluated with respect to full Monte-Carlo simulations. Figure 15 shows the results of a Monte-

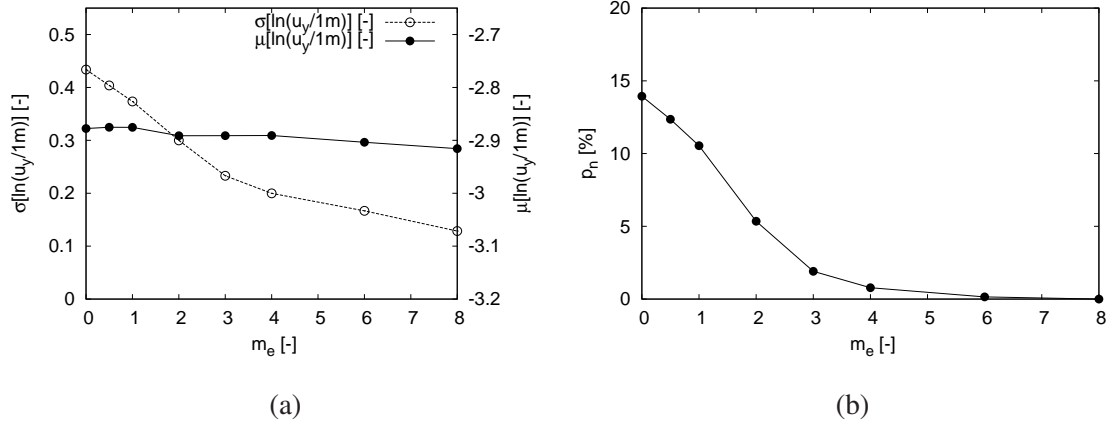


Figure 14: (a) The dependency of the mean value and standard deviation of $\ln(u_y/1m)$ on m_e ; (b) the dependency of the probability of unsatisfactory performance due to natural variability and experimental uncertainty p_n on m_e .

Carlo simulation with 7000 realisations for $n_t = 37$, $n_e = 40$ and $m_e = 1$. The Monte-Carlo and FOSM simulation results practically coincide.

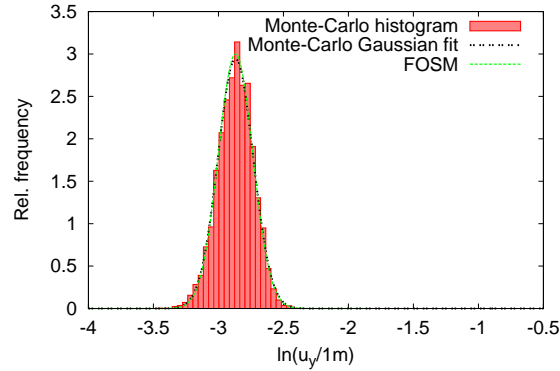


Figure 15: Comparison of Monte-Carlo and FOSM simulations revealing sampling uncertainty ($n_t = 37$, $n_e = 40$, $m_e = 1$).

When $\sigma_s[Y]$ (standard deviation of the performance function due to sampling uncertainty) is calculated using the FOSM method, the total variance of Y can be calculated using Eq. (23), which can then be used in the evaluation of the probability of unsatisfactory performance due to natural variability and experimental and sampling uncertainties, denoted as p_{ns} . In the present case of $n_t = 37$, $n_e = 40$ and $m_e = 1$, $p_{ns} = 11.9\%$. When compared with $p_n = 10.5\%$, it can be seen that the sampling uncertainty increases the probability of unsatisfactory performance; for the current sample size the effect is, however, not substantial.

The relatively small effect of sampling uncertainty on p_{ns} is caused by the number of samples

$n_t = 37$ and $n_e = 40$, which is relatively high for standard practical projects. To understand the influence of n_e and n_t , two additional sets of FOSM simulations were run. In one set, n_t was kept constant at a high value of $n_t = 80$ and n_e was varied. In the second set, $n_e = 80$ and n_t was varied. In the simulations, the values $\hat{\mu}[X_i]$ and $\hat{\sigma}[\varepsilon_n[X_i]]$ were kept constant. The results of these simulations are shown in Figs. 16a and b. n_e has a small effect on p_{ns} even at the relatively low value of $n_e = 5$. In contrast, the effect of n_t is more substantial, influencing simulation results significantly for $n_t < 40$. This is because the tests on total variability are needed to specify both the mean value and variance of a parameter, whereas the tests on experimental uncertainty define variance only. It can be concluded that, in practical projects, an effort should be put into sampling for total variability, while the experimental uncertainty may be quantified using a relatively low number of samples.

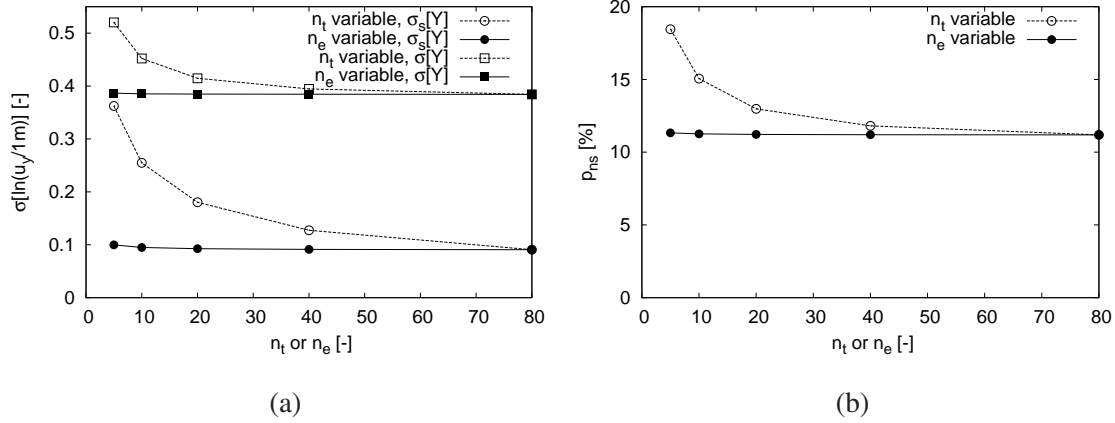


Figure 16: (a) The dependency of the standard deviation of $\ln(u_y/1m)$ (sampling only $\sigma_s[Y]$ and total $\sigma[Y]$) on the number of samples; (b) the dependency of the probability of unsatisfactory performance p_{ns} on the number of samples.

Summary and conclusions

An approach to quantify the effects of experimental and sampling uncertainties has been developed in this paper. The application of the proposed approach has been demonstrated by simulating the displacement of a foundation on a spatially variable sandy soil. Two extensive data sets were obtained by testing 37 samples revealing the effect of total variability and 40 samples revealing the effect of experimental uncertainty. It was demonstrated that the experimental uncertainty represents a substantial fraction of the measured total variability.

Counter-intuitively, it has been shown that an increase in experimental uncertainty *for the given total variability* measured on spatially variable samples decreases the calculated probability of un-

satisfactory performance. It has been argued that this is possibly a reason for the relatively common overestimation of the probability of unsatisfactory performance in geotechnical engineering probabilistic simulations. By evaluating the sampling uncertainty it was found that while a relatively large number of samples ($n_t > 40$) is needed to properly characterise the total variability, a much smaller number of samples ($n_e > 5$) is sufficient for the experimental uncertainty quantification.

Considering that no software adjustments are needed for the incorporation of experimental uncertainty into existing codes based on random field methods, and that relatively little additional experimental effort is needed for experimental uncertainty quantification, it is recommended that a consideration of experimental uncertainty should become more common in geotechnical engineering probabilistic analyses.

Acknowledgment

Financial support by the research grant GACR P105/12/1705 is greatly appreciated. The tests quantifying the experimental uncertainty were performed by P. Mayer within his MSc project. The author is grateful to doc. J. Ježek, doc. Z. Hlávka and to J. Ondřej for valuable discussions on the manuscript.

References

- Akbas, S. O. & Kulhawy, F. H. (2010). Characterisation and estimation of geotechnical variability in Ankara clay: A case history. *Geotech Geol Eng* **28**, 619–631.
- Al-Naqshabandy, M. S. & Larsson, S. (2013). Effect of uncertainties of improved soil shear strength on the reliability of embankments. *Journal of Geotechnical and Geoenvironmental Engineering ASCE* **139**, No. 4, 619–632.
- Andrade, J. E., Baker, J. W. & Ellison, K. C. (2008). Random porosity fields and their influence on the stability of granular media. *International Journal for Numerical and Analytical Methods in Geomechanics* **32**, 1147–1172.
- Bauer, E. (1996). Calibration of a comprehensive constitutive equation for granular materials. *Soils and Foundations* **36**, No. 1, 13–26.
- Booy, C. & Lye, L. M. (1989). A new look at flood risk determination. *Water Resources Bulletin* **25**, No. 5, 933–943.
- Bourdeau, P. L. & Amundaray, J. I. (2005). Non-parametric simulation of geotechnical variability. *Géotechnique* **55**, No. 2, 95–108.

- Brzakała, W. & Puła, W. (1996). A probabilistic analysis of foundation settlements. *Computers and Geotechnics* **18**, No. 4, 291–309.
- Castrup, H. (2004). Estimating and combining uncertainties. In *8th Annual ITEA Instrumentation Workshop, Lancaster CA*.
- Cho, S. E. (2007). Effect of spatial variability of soil properties on slope stability. *Engineering Geology* **92**, 97–109.
- Cho, S. E. & Park, H. C. (2010). Effect of spatial variability of cross-correlated soil properties on bearing capacity of strip footing. *International Journal for Numerical and Analytical Methods in Geomechanics* **34**, 1–26.
- Christian, J. T. & Baecher, G. B. (1999). Point-estimate method as numerical quadrature. *Journal of Geotechnical and Geoenvironmental Engineering ASCE* **125**, No. 9, 779–786.
- Christian, J. T., Ladd, C. C. & Baecher, G. B. (1994). Reliability applied to slope stability analysis. *Journal of Geotechnical Engineering ASCE* **120**, No. 12, 2180–2207.
- DeGroot, D. J. & Baecher, G. B. (1993). Estimating autocovariance of in-situ soil properties. *Journal of Geotechnical Engineering* **119**, No. 1, 147–166.
- Duncan, J. M. (2000). Factors of safety and reliability in geotechnical engineering. *Journal of Geotechnical and Geoenvironmental Engineering ASCE* **126**, No. 4, 307–316.
- El Gonnouni, M., Riou, Y. & Hicher, P. Y. (2005). Geostatistical method for analysing soil displacement from underground urban construction. *Géotechnique* **55**, No. 2, 171–182.
- El-Ramly, H., Morgenstern, N. R. & Cruden, D. M. (2002). Probabilistic slope stability analysis for practice. *Canadian Geotechnical Journal* **39**, 665–683.
- El-Ramly, H., Morgenstern, N. R. & Cruden, D. M. (2005). Probabilistic assessment of stability of a cut slope in residual soil. *Géotechnique* **55**, No. 1, 77–84.
- El-Ramly, H., Morgenstern, N. R. & Cruden, D. M. (2006). Lodalen slide: a probabilistic assessment. *Canadian Geotechnical Journal* **43**, No. 9, 956–968.
- Elkateb, T., Chalaturnyk, R. & Robertson, P. K. (2003). An overview of soil heterogeneity: quantification and implications on geotechnical field problems. *Canadian Geotechnical Journal* **40**, No. 1, 1–15.
- Fenton, G. A. (1997). Probabilistic methods in geotechnical engineering. In *Workshop presented at ASCE GeoLogan'97 conference, Logan, Utah*.

- Fenton, G. A. & Griffiths, D. V. (2002). Probabilistic foundation settlement on a spatially random soil. *Journal of Geotechnical and Geoenvironmental Engineering ASCE* **128**, No. 5, 381–390.
- Fenton, G. A. & Griffiths, D. V. (2003). Bearing-capacity prediction of spatially random c - ϕ soils. *Canadian Geotechnical Journal* **40**, 64–65.
- Fenton, G. A. & Griffiths, D. V. (2005). Three-dimensional probabilistic foundation settlement. *Journal of Geotechnical and Geoenvironmental Engineering ASCE* **131**, No. 2, 232–239.
- Frey, H. C. (1993). Separating variability and uncertainty in exposure assessment: motivation and methods. In *86th Annual Meeting of the Air and Waste Management Association, Paper No. 93-79.01*.
- Griffiths, D. V. & Fenton, G. A. (2004). Probabilistic slope stability analysis by finite elements. *Journal of Geotechnical and Geoenvironmental Engineering ASCE* **130**, No. 5, 507–518.
- Griffiths, D. V., Fenton, G. A. & Manoharan, N. (2002). Bearing capacity of rough rigid strip footing on cohesive soil: probabilistic study. *Journal of Geotechnical and Geoenvironmental Engineering ASCE* **128**, No. 9, 743–755.
- Hájek, V., Mašín, D. & Boháč, J. (2009). Capability of constitutive models to simulate soils with different OCR using a single set of parameters. *Computers and Geotechnics* **36**, No. 4, 655–664.
- Hald, A. (1951). *Statistical theory with engineering applications*. John Wiley and Sons, New York.
- Haldar, S. & Babu, G. L. S. (2008). Effect of soil spatial variability on the response of laterally loaded pile in undrained clay. *Computers and Geotechnics* **35**, 537–547.
- Head, K. H. (1985). *Manual of soil laboratory testing. volume 3: Effective stress tests*. John Wiley and Sons, Chichester.
- Helton, J. C. (1997). Uncertainty and sensitivity analysis in the presence of stochastic and subjective uncertainty. *Journal of Statistical Computation and Simulation* **57**, 3–76.
- Herle, I. & Gudehus, G. (1999). Determination of parameters of a hypoplastic constitutive model from properties of grain assemblies. *Mechanics of Cohesive-Frictional Materials* **4**, 461–486.
- Hicks, M. A. & Onisiphorou, C. (2005). Stochastic evaluation of static liquefaction in a predominantly dilative sand fill. *Géotechnique* **55**, No. 2, 123–133.
- Hicks, M. A. & Samy, K. (2002). Influence of heterogeneity on undrained clay slope stability. *Quarterly Journal of Engineering Geology* **35**, 41–49.

- Hofer, E., Kloos, M., Krzykacz-Hausmann, B., Peschke, J. & Woltereck, M. (2002). An approximate epistemic uncertainty analysis approach in the presence of epistemic and aleatory uncertainties. *Reliability Engineering and System Safety* **77**, 229–238.
- Hsu, S.-C. & Nelson, P. P. (2006). Material spatial variability and slope stability of weak rock masses. *Journal of Geotechnical and Geoenvironmental Engineering ASCE* **132**, No. 2, 183–193.
- Huber, M., Vermeer, P. A. & Bárdossy, A. (2010). Evaluation of soil variability and its consequences. In *Proc. 7th European Conference on Numerical Methods in Geomechanics (NUMGE), Trondheim, Norway* (Benz, T. & Nordal, S., eds.), Taylor & Francis Group, London, pp. 363–368.
- Jáky, J. (1944). The coefficient of earth pressure at rest. *Journal for Society of Hungarian Architects and Engineers* , 355–357.
- Jung, B.-C., Gardoni, P. & Biscontin, G. (2008). Probabilistic soil identification based on cone penetration tests. *Géotechnique* **58**, No. 7, 591–603.
- Kim, B. S. N. (2002). Probabilistic analysis of settlement for a floating foundation on soft clay. *KSCCE Journal of Civil Engineering* **6**, No. 2, 235–241.
- Kim, H.-K. & Santamarina, J. C. (2008). Spatial variability: drained and undrained deviatoric load response. *Géotechnique* **58**, 805–814.
- Lumb, P. (1966). The variability of natural soils. *Canadian Geotechnical Journal* **3**, No. 2, 74–97.
- Mašín, D. (2012). Asymptotic behaviour of granular materials. *Granular Matter* **14**, No. 6, 759–774.
- Mayer, P. (2013). *Evaluation of the variability of mechanical parameters of coarse-grained soils (in Czech)*. Master's thesis, Charles University in Prague, Czech Republic.
- Merz, B. & Thieken, A. H. (2005). Separating natural and epistemic uncertainty in flood frequency analysis. *Journal of Hydrology* **309**, 114–132.
- Müller, R., Larsson, S. & Spross, J. (2014). Extended multivariate approach for uncertainty reduction in the assessment of undrained shear strength in clays. *Canadian Geotechnical Journal* **51**, 231–245.
- Niemunis, A., Wichtmann, T., Petryna, Y. & Triantafyllidis, T. (2005). Stochastic modelling of settlements due to cyclic loading for soil-structure interaction. In *Proceedings of the 9th International Conference on Structural Safety and Reliability, ICOSSAR'05, Rome, Italy* (Augusti, G., Schuëller, G. & Ciampoli, M., eds.), Millpress, Rotterdam.

- Nour, A., Slimani, A. & Laouami, N. (2002). Foundation settlement statistics via finite element analysis. *Computers and Geotechnics* **29**, 641–672.
- Nübel, K. & Karcher, C. (1998). FE simulations of granular material with a given frequency distribution of voids as initial condition. *Granular Matter* **1**, 105–112.
- Oberguggenberger, M. & Fellin, W. (2008). Reliability bounds through random sets: Non-parametric methods and geotechnical applications. *Computers and Structures* **86**, 1093–1101.
- Peschl, G. M. & Schweiger, H. F. (2003). Reliability analysis in geotechnics with finite elements - Comparison of probabilistic, stochastic and fuzzy set methods. In *Proc. 3rd int. symposium on imprecise probabilities and their applications*, Canada: Carleton Scientific, pp. 437–451.
- Phoon, K.-K. & Kulhawy, F. H. (1999a). Characterisation of geotechnical variability. *Canadian Geotechnical Journal* **36**, 612–624.
- Phoon, K.-K. & Kulhawy, F. H. (1999b). Evaluation of geotechnical property variability. *Canadian Geotechnical Journal* **36**, 625–639.
- Popescu, R., Prevost, J. H. & Deodatis, G. (1997). Effects of spatial variability on soil liquefaction: some design recommendations. *Géotechnique* **47**, No. 5, 1019–1036.
- Rodemann, D. (2008). *Tochnog professional user's manual*. <http://www.feat.nl>.
- Rosenblueth, E. (1981). Two-point estimates in probabilities. *Appl. Math. Modelling* **5**, No. 2, 329–335.
- Schumacher, B. A., Shines, K. C. & Burton, J. V. (1990). Comparison of three methods for soil homogenization. *Soil Sci. Soc. Am. J.* **54**, No. 4, 1187–1190.
- Schweiger, H. F. & Peschl, G. M. (2005). Reliability analysis in geotechnics with a random set finite element method. *Computers and Geotechnics* **32**, 422–435.
- Smith, T. E. (2014). *Notebook on spatial data analysis [online]*. <http://www.seas.upenn.edu/~ese502>.
- Soulié, M., Montes, P. & Silvestri, V. (1990). Modelling spatial variability of soil parameters. *Canadian Geotechnical Journal* **27**, 617–630.
- Suchomel, R. & Mašín, D. (2010). Comparison of different probabilistic methods for predicting stability of a slope in spatially variable c-phi soil. *Computers and Geotechnics* **37**, 132–140.
- Suchomel, R. & Mašín, D. (2011). Probabilistic analyses of a strip footing on horizontally stratified sandy deposit using advanced constitutive model. *Computers and Geotechnics* **38**, No. 3, 363–374.

- Sun, S., Fu, G., Djordjević, S. & Khu, S.-T. (2012). Separating aleatory and epistemic uncertainties: Probabilistic sewer flooding evaluation using probability box. *Journal of Hydrology* **420-421**, 360–372.
- Tatsuoka, F., Iwasaki, T., Yoshida, S., Fukushima, S. & Sudo, H. (1979). Shear modulus and damping by drained tests on clean sand specimens reconstituted by various methods. *Soils and Foundations* **19**, 39–54.
- Uzielli, M., Vannucchi, G. & Phoon, K. K. (2005). Random field characterisation of stress-normalised cone penetration testing parameters. *Géotechnique* **55**, No. 1, 3–20.
- Vanmarcke, E. H. (1983). *Random fields: analysis and synthesis*. M.I.T. press, Cambridge, Mass.
- von Wolffersdorff, P. A. (1996). A hypoplastic relation for granular materials with a predefined limit state surface. *Mechanics of Cohesive-Frictional Materials* **1**, No. 3, 251–271.
- Wang, Y.-J. & Chiasson, P. (2006). Stochastic stability analysis of a test excavation involving spatially variable subsoil. *Canadian Geotechnical Journal* **43**, 1074–1087.
- Watabe, Y., Shiraishi, Y., Murakami, T. & Tanaka, H. (2007). Variability of physical and consolidation test results for relatively uniform clay samples retrieved from Osaka bay. *Soils and Foundations* **47**, No. 4, 701–716.
- Wichtmann, T. & Triantafyllidis, T. (2012). Behaviour of granular soils under environmentally induced cyclic loads. In *Behaviour of granular soils under environmentally induced cyclic loads*, CISM International Centre for Mechanical Sciences, Springer.
- Wu, Z., Tang, H., Wang, S. & Ge, X. (2013). Influence of number of geotechnical samples on slope reliability analysis. *Chinese Journal of Rock Mechanics and Engineering* **32**, 2846–2854.
- Zhao, H. F., Zhang, L. M., Xu, Y. & Chang, D. S. (2013). Variability of geotechnical properties of a fresh landslide soil deposit. *Engineering Geology* **166**, 1–10.
- Zhou, J. & Nowak, A. S. (1988). Integration formulas to evaluate functions of random variables. *Structural Safety* **5**, 267–284.